CHAPTER 6

6. APPLICATION OF THE FE MODEL FOR CAPPING LAYER IN PRACTICE

6.1 Introduction

The preceding Chapters have demonstrated the development of a FE model based backcalculation process to predict the properties of the capping layer material coupled with the testing of the soil specimens in semi confined condition using CBR mould. The predicted properties have been shown to lie within the range of the expected values and/or the values reported in the literature for similar materials. Prior to applying the FE model based backcalculation process and the associated Semi Confined Tests (SCT) for practical cases, it is necessary to show the process is robust enough, especially for changes to boundary conditions. This is especially important as the SCT specimens were subjected to extreme levels of lateral stresses due to the rigid boundaries of the CBR mould.

The capping layer of railway subgrade, however, will normally not have such rigid lateral boundaries and hence under vertical penetration (for example, due to ballast pocket formation mechanism) their behaviour might differ to that of the specimens tested using SCT process. Furthermore, the SCT specimens have had axi-symmetric response whilst most rail tracks are normally analysed using plane strain idealisation. Therefore, it was necessary to examine the behaviour of the capping layer with reduced level of lateral confinement under plane strain condition by suitably modifying the FE model developed in Chapters 4 and 5. It was also necessary to carry out verification tests to validate the predictions of the modified FE model.

Basically, capping layers act to improve subgrade load bearing capability by protecting weak underlying layers that may prevail in the natural conditions. Given that all the deformations during construction and operation of the railway lines will be focussed on the behaviour of the cross sectional planes yz shown in Fig. 6.1, a plane strain model is most appropriate. The major (σ_1) and minor (σ_3) principal stresses occur in these cross sectional planes while the intermediate (σ_2) principal stress is parallel to the x-axis.

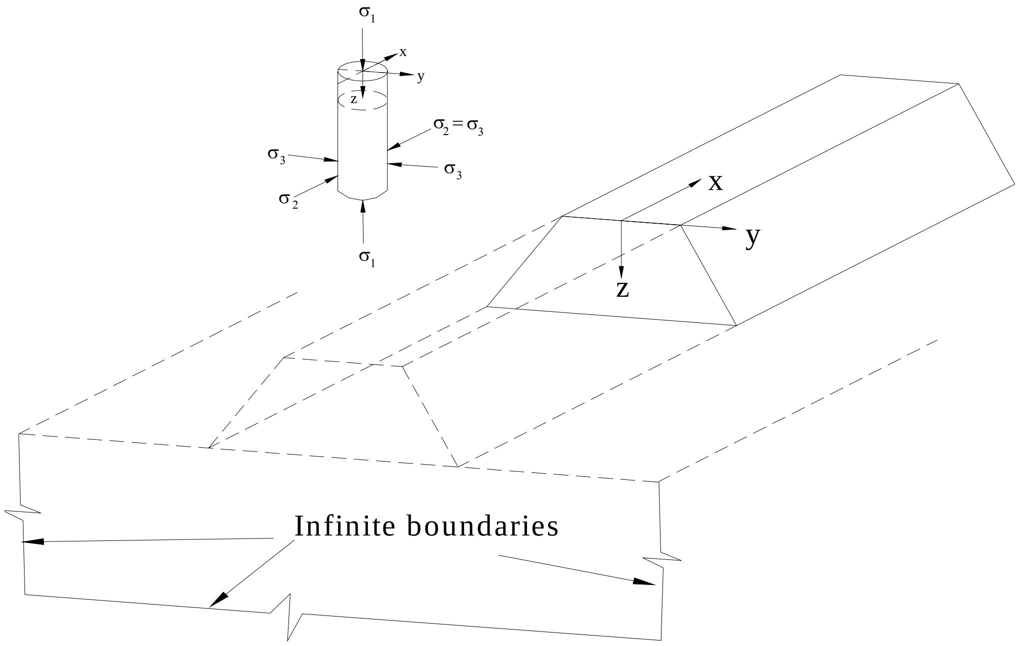

Figure 6.1 Plane strain conditions in a railway embankment

In order to validate that the results from the proposed technique described in Chapters 3, 4 and 5 are representative of the in-service performance of the capping layer material in railway subgrade, further modifications to the FE model as well as validation experiments under plane strain conditions are required. In order to keep the whole process much simpler, it is prudent to consider only the capping layer in the FE modelling and analysis although the capping layer in practice is sandwiched between several other layers of complex materials.

It should be noted that the major objective of the thesis is to develop an economical method of testing and establishing a process for calculating the properties of the capping layer material only, and not to involve detailed analysis of the rail track behaviour. *It is believed the procedure developed in the thesis to characterise the materials using a simpler testing process coupled with FE modelling based backcalculation can be used for any material used in track construction and the properties predicted could then be used in the analysis of track substructures*.

This Chapter presents the modified FE model, its predictions of the behaviour of capping layer under plane strain conditions subjected to vertical penetration and the validation of such predictions. The corresponding data relevant to this Chapter are located in Appendices D.1-D.3.

APPENDIX D.1	Convergence studies of the plane strain FE model
APPENDIX D.2	Application of SCT predicted properties to the plane strain FEM
APPENDIX D.3	Large-scale experiments data sheets

6.2 Design of Experiments for Plane Strain Conditions

To facilitate the testing of the capping layer material under plane strain conditions with much reduced levels of confining stress, a large scale experimental setup was designed. This required testing of a large volume of the capping layer material. Furthermore, as final validation experiments were sought, the large volume testing was required to be carefully designed by considering the constraints of costs, time and the laboratory limitations on space and loading/ deformation levels. The size of the box was selected to accommodate low levels of lateral stresses. The design has resulted in rigid steel boxes of internal dimensions 1.6m x 1.6m x 1.2m. The box consisted of 32mm thick base plate, 6mm thick walls with 12 mm thick vertical gussets in two opposite sides, and 10mm thick vertical and horizontal gussets in the other two opposite sides of which one was designed with a 10mm thick clear polycarbonate sheet for viewing purposes (Fig. 6.2).

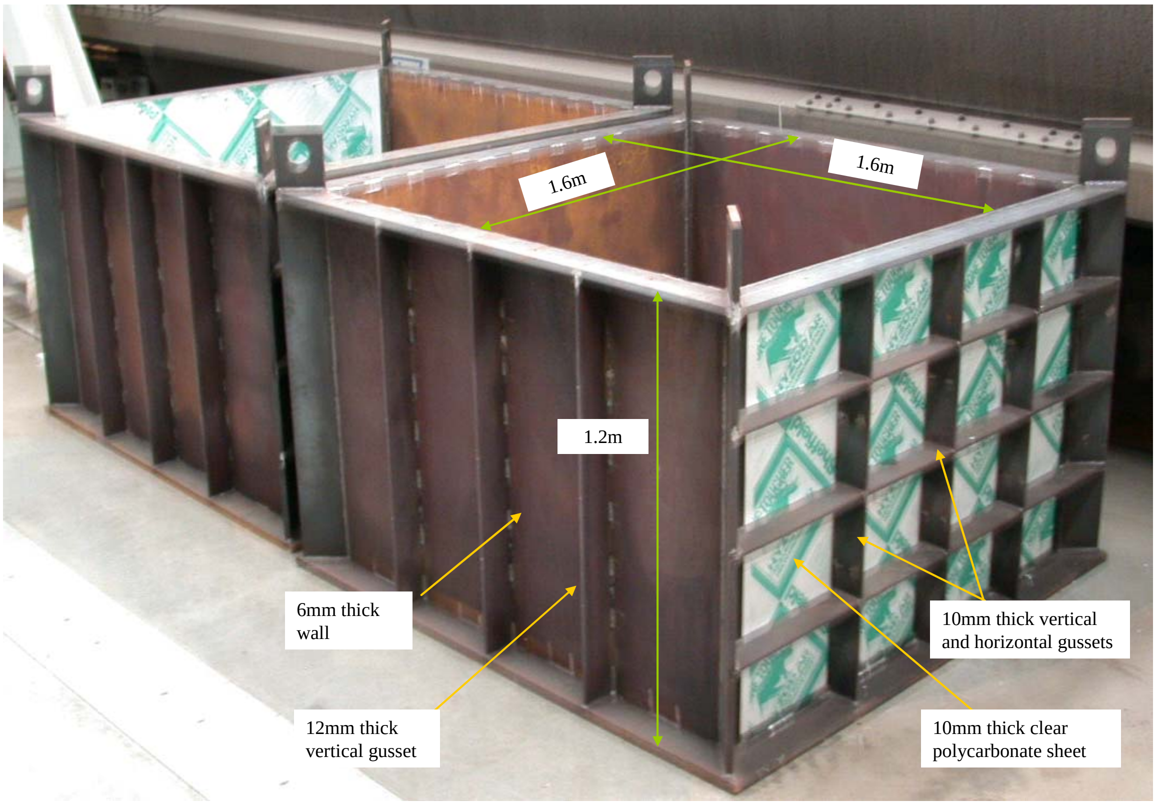

Figure 6.2 Boxes used for the testing of large scale capping layer material

Capping layer thicknesses recommended for improvement of in-situ conditions are often in the range from 300 to 600mm. Therefore, two thicknesses of the capping layer material were considered in the validation tests; 300 and 600mm.

Design of loading plate

A loading plate of 350mm x 700mm was considered large enough not to cause excessive stresses and small enough not to distribute the imposed loading to the side walls of the boxes. The length to width ratio of the loading plate was kept as two primarily to ensure that the load was transferred as a strip load incorporating the plane strain conditions sought in the FE model. Secondly it ensured that the effect of load transferred through the soil mass to the vertical faces of the box would be minimal based on a vertical load spread slope of 1:1 (Fig. 2.11). In order to achieve a uniform load distribution over the entire plate area, a stack of 50mm thick plates were also designed to transfer the load uniformly to the specimen as shown in Fig. 6.3 (a), (b) and (c).

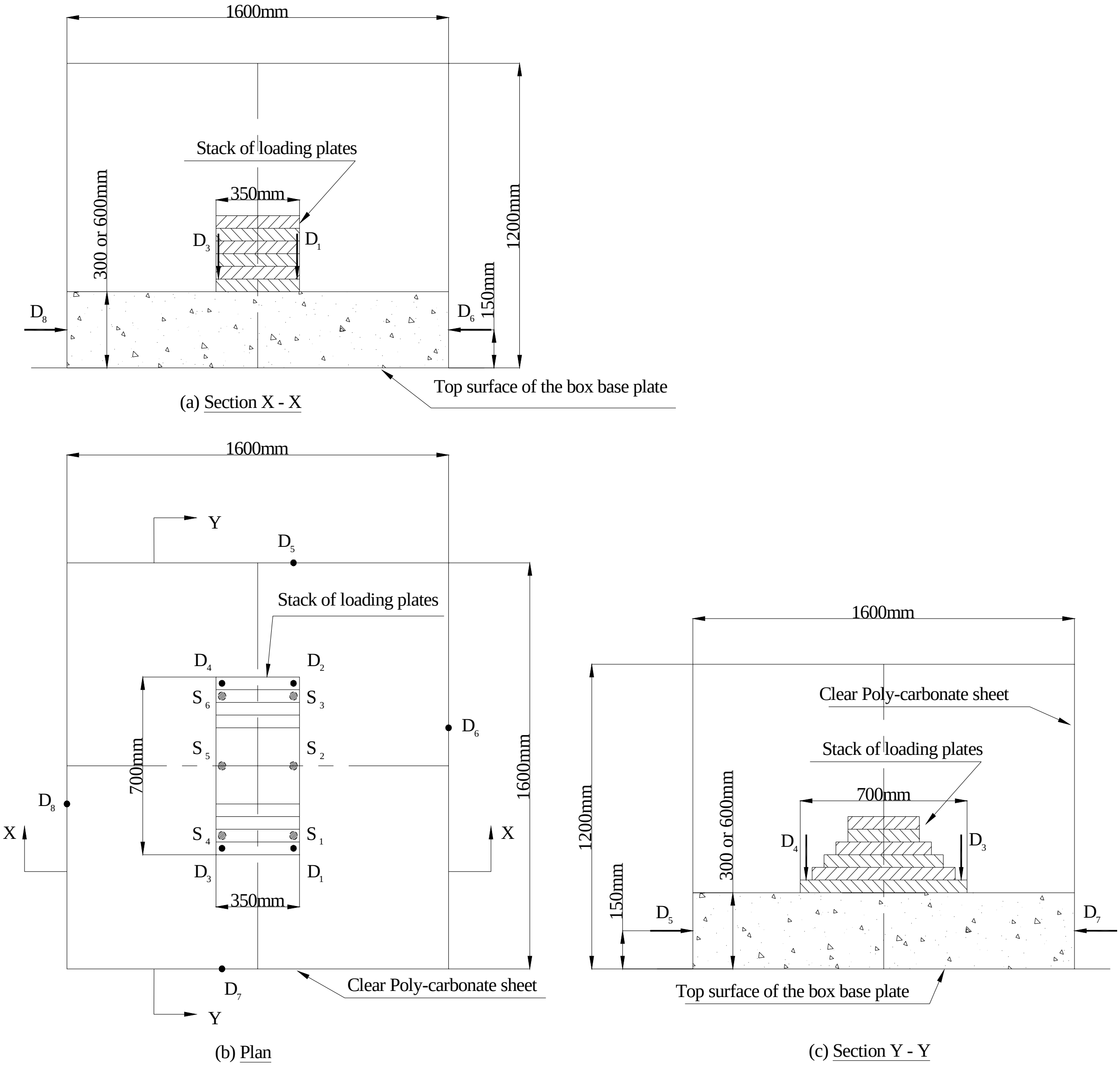

Note:
D denotes displacement transducers and S denotes strain gauges
Only the internal dimensions of the box are shown for clarity

Figure 6.3 Load distribution method and instrumentation layout

Design of Instrumentation

To obtain reliable results desired from the experimental investigations, it was required to locate all instrumentation independent of the box or the loading frame. An independent framework was therefore designed to hold the displacement transducers and the framework was attached to the concrete floor. The vertical deformation of the specimens was measured using two sets of displacement transducers D_1/D_3 and D_2/D_4 at the corners of the bottom plate shown in Fig. 6.3 (b) and the average displacement of these transducers were taken as the deformation of the capping layer. Another two sets of displacement transducers, D_5/D_7 and D_6/D_8 on the walls shown in Fig. 6.3 (b) were used to measure any horizontal movements during loading. The displacement transducers D_5/D_7 and D_6/D_8 were located at 150mm above the bottom plate of the box as depicted in Fig. 6.3 (a) and (c).

As shown in Fig. 6.3 (b), by locating three sets of strain gauges S_1/S_4, S_2/S_5 and S_3/S_6 on the bottom plate, any uneven movements due to warping or bending of the plate during loading were measured.

Method of compaction

In practice, capping layers are compacted in horizontal layers *not exceeding* 200mm loose thickness and the minimum density to be achieved is 95% of the maximum dry density by modified compaction.

Thus, in order to achieve the required uniform density in the experiments it was decided to compact the material in horizontal layers of 150mm thickness. To ensure that a uniform density was achieved in each layer, a pre-calculated mass of the required volume was used for each layer. Given the limited work space within the box it was necessary to use a small 40kg plate compactor of plate size 420 x 292mm for the compaction of the material. It was also decided to measure the as-compacted density by weighing the compacted material boxes just after compaction and to measure the moisture content using a small portion of the material sample used. At the completion of the test the density of the samples was measured using a Surface Moisture-Density Gauge (SMDG).

6.3 FE Modelling of the Capping Layer under Plane Strain Conditions

6.3.1 FE Model

The capping layer material modelled as a plane strain problem is illustrated in Fig. 6.4. The model in ABAQUS/Explicit used 4-node plane strain quadrilateral elements (CPE4R) with reduced integration. A suitable mesh was adopted after convergence studies using several trials of mesh densities. The bottom of the sample was restrained in direction 2 while the two vertical sides were restrained in direction 1. An analytical rigid surface was used to define the loading plate, positioned in contact with the top edge of the soil sample. The rigid surface was constrained to translate vertically downwards through a pre-defined displacement history. The displacement of the rigid surface was defined using the AMPLITUDE option using the SMOOTH STEP sub-option. The surface-to-surface contact between the rigid surface and the soil sample was defined using the finite sliding KINEMATIC based contact algorithm with contact pairs. Hard contact was defined in the vertical direction while a frictionless contact was defined in the tangential direction. ADAPTIVE MESH control option was used to avoid mesh distortion. The analysis was performed using ABAQUS/Explicit and the VUMAT routine was called at each material calculation point.

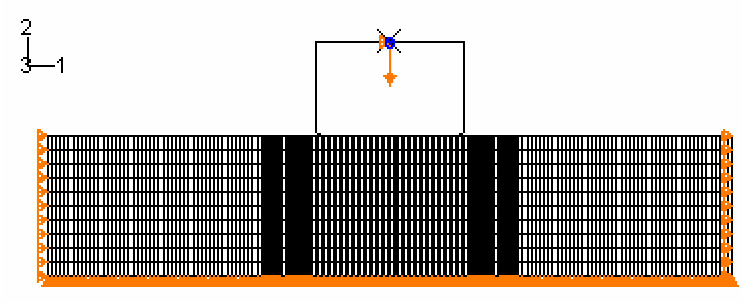

(a) 300mm layer model

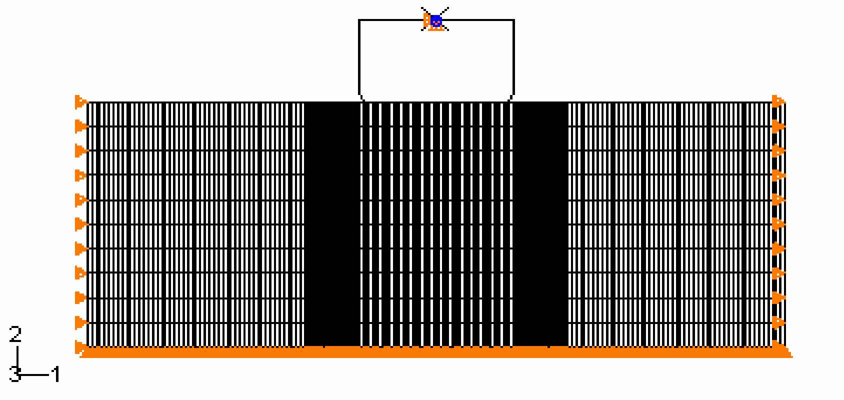

(b) 600mm layer model

Figure 6.4 ABAQUS plane strain model

6.3.2 *Mesh Convergence Studies*

As before, a mesh refinement was carried out to assess the sensitivity of the model predictions to the mesh density. Figs. 6.5 and 6.6 show three different mesh densities used in 300 and 600mm thick layers respectively.

Fig. 6.7 shows load-displacement profiles obtained, indicating that the medium meshes predicted similar results to that of fine meshes. Therefore the medium density meshes were used for both 300mm and 600mm layer specimens in the simulations for optimising the CPU time (Table 6.1). The coarse meshes were avoided due to noisy results. The relevant FE analysis data are given in Appendix D.1.

Table 6.1 Mesh refinement results

	300mm layer			600mm layer		
Mesh density	Coarse	Medium	Fine	Coarse	Medium	Fine
Mesh size	10x36	10x200	10x360	15x60	10x200	10x360
Number of elements	360	2000	3600	976	2000	3600
Number of nodes	407	2211	3971	900	2211	3971
CPU Time (hrs:min:sec)	00:00:03	00:00:44	00:02:46	00:00:08	00:00:41	00:02:31

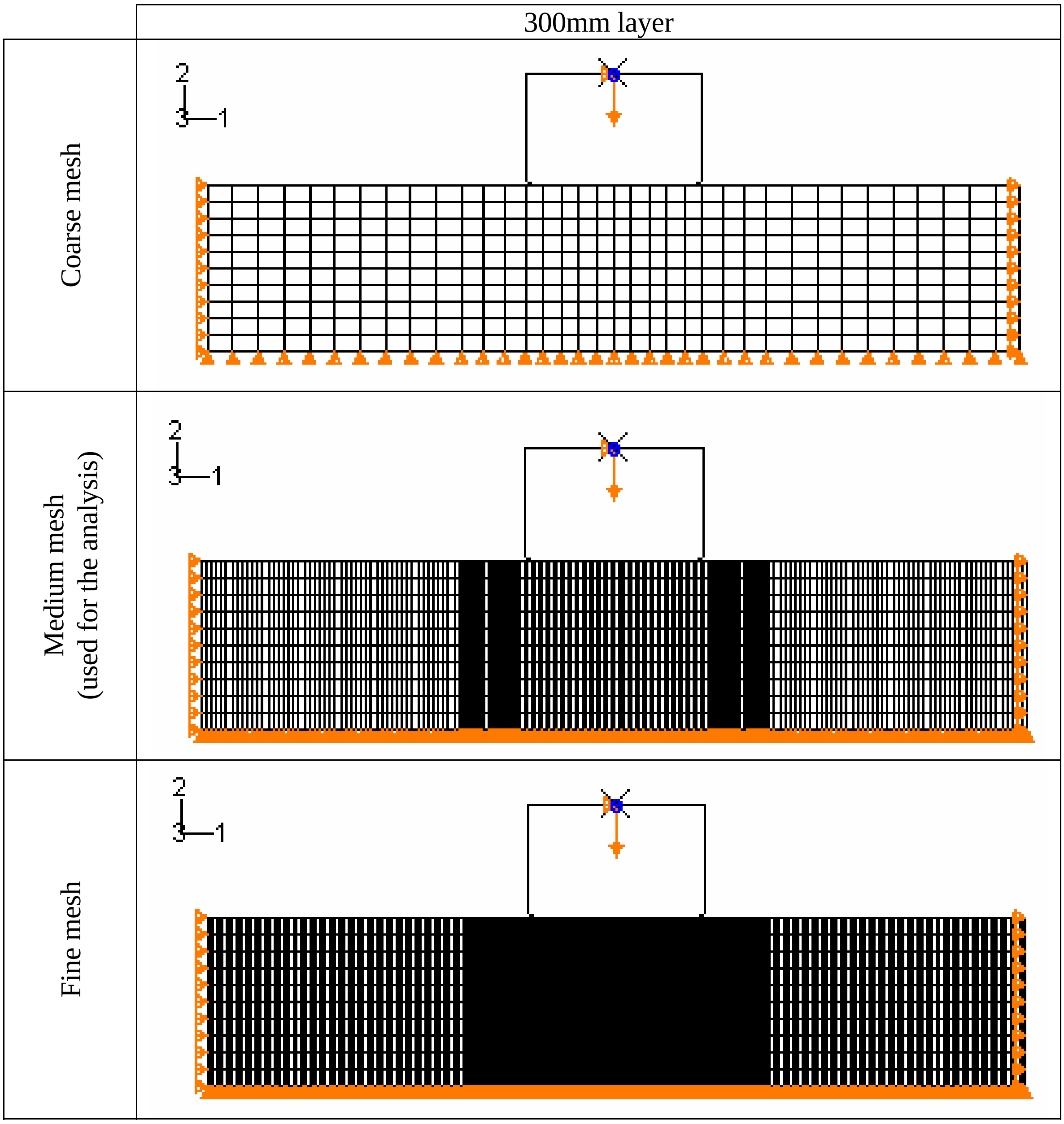

Figure 6.5 Original mesh configurations at different mesh densities of 300mm layer

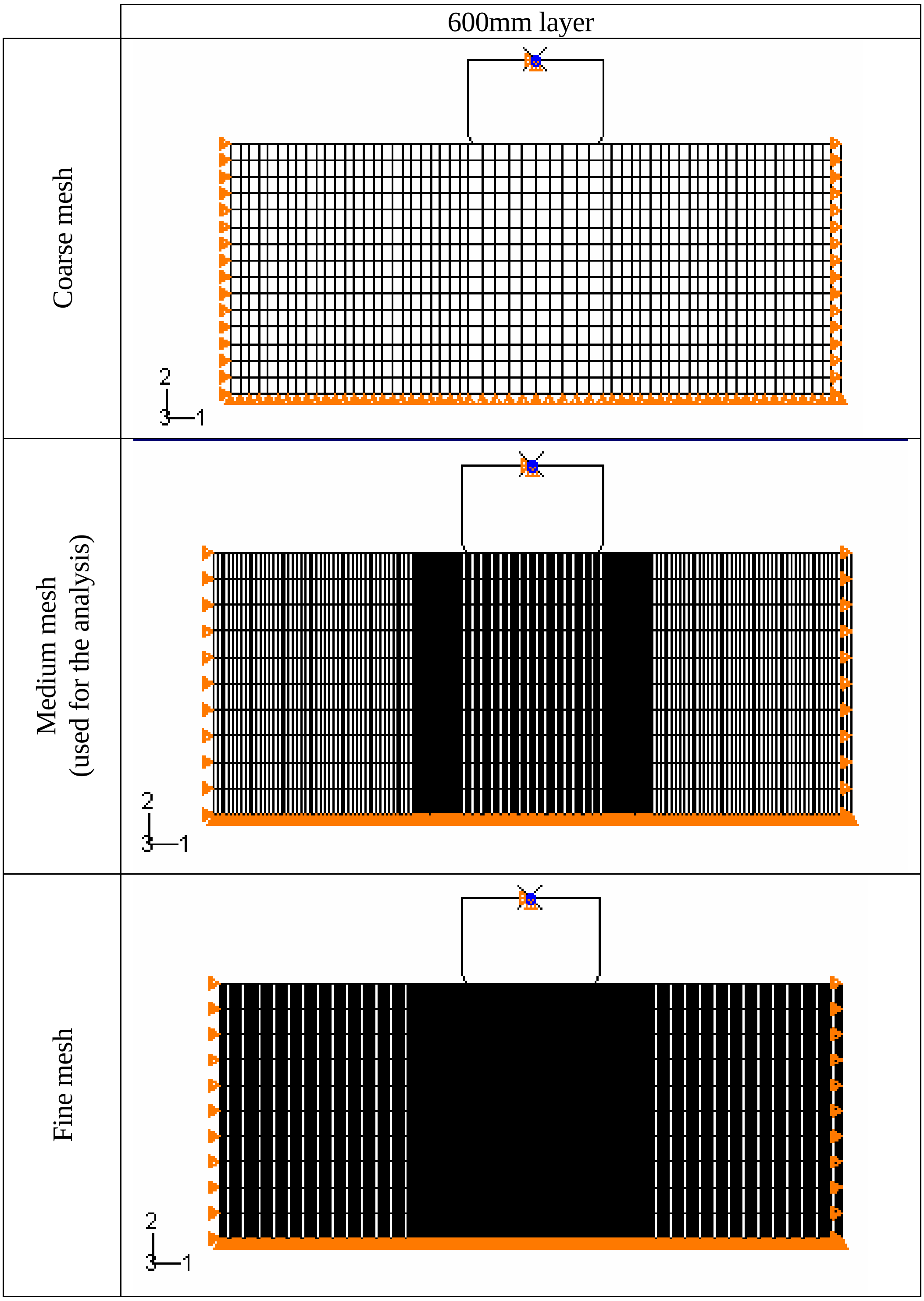

Figure 6.6 Original mesh configurations at different mesh densities of 600mm layer

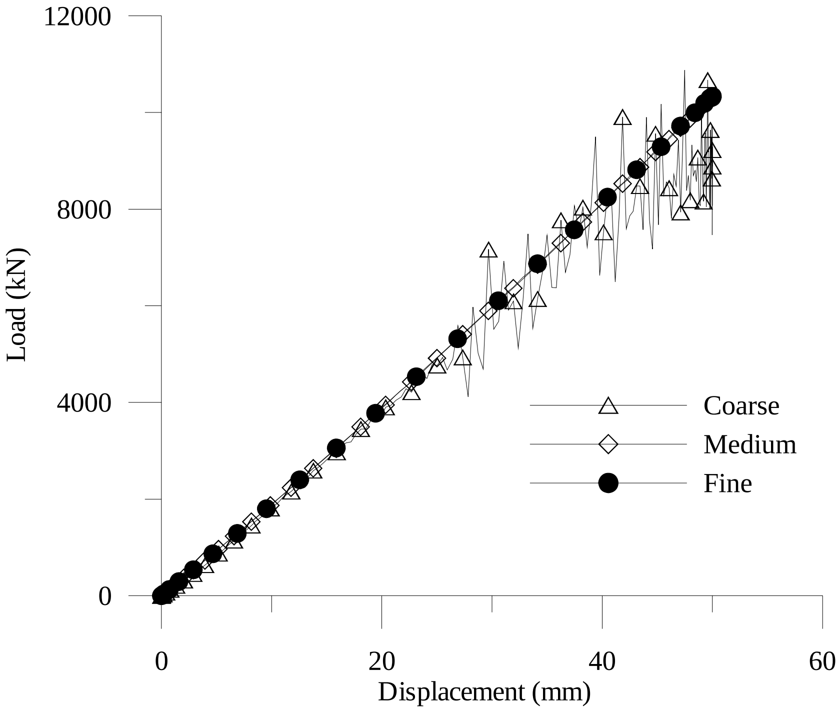

(a) 300mm layer

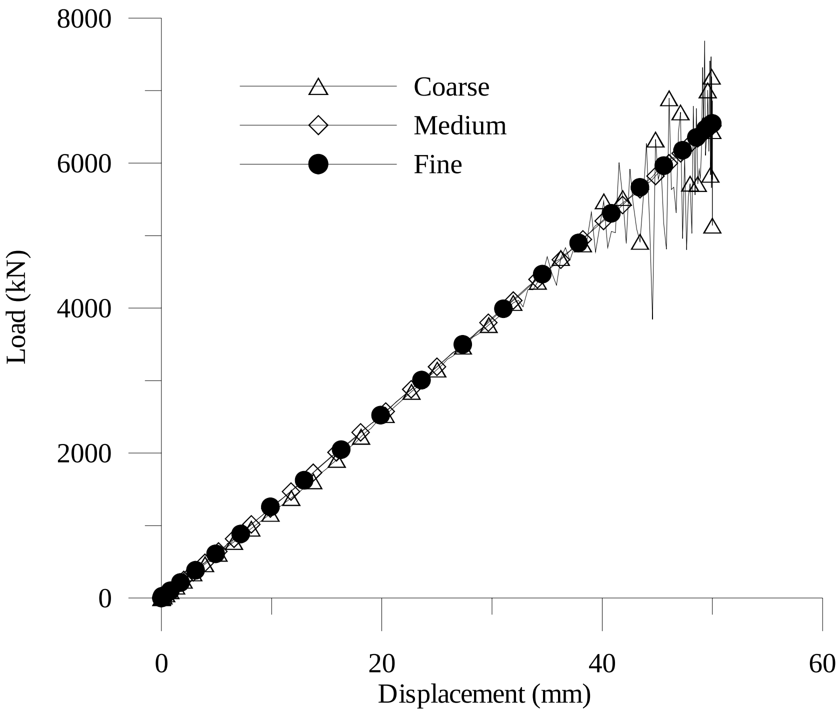

(b) 600mm layer

Figure 6.7 Load-displacement profiles of the large-scale set-up, ABAQUS/Explicit; influence of mesh refinement

6.3.3 Analysis, Results and Discussions

The purpose of the analysis was to demonstrate that the material data obtained from the axisymmetric FE modelling based backcalculation coupled with the semi confined tests could be used for the prediction of the capping layer behaviour under plane strain condition with much reduced level of lateral confinement. Although the axisymmetric analyses were carried out for specimens containing three different moisture levels, it was decided to carry out the plane strain analyses for only specimens under OMC condition. The material data obtained from the axisymmetric model for OMC state (Table 6.2) were used in the analysis of the plane strain model of the capping layer material.

Table 6.2 Model predictions of SCT setup for OMC state

		Elastic			Plastic	
		$E_0 \le E_t \le E_{max}$ (MPa)	$\phi_{min} \le \phi \le \phi_{max}$ (^{0})	c (kPa)	ψ (^{0})	H_p (kPa)
OMC	Lower bound	$30 \le E_t \le 80$	$35 \le \phi \le 38$	300	4	300
	Upper bound	$80 \le E_t \le 130$	$35 \le \phi \le 38$	350	7	350

The relevant FE analysis data sheets are located in Appendix D.2.

Fig. 6.8 (a) and (b) show the plane strain model predictions for upper and lower bounds obtained from the analysis respectively. It can be seen from the graphs that the 300mm layer showed an initial stiffer response than the 600mm layer. This has changed in the upper bound response beyond 15mm deformation where the 600mm layer started to gain a stiffer response while the 300mm layer started to show some failure with the increase in imposed penetration. At the lower bound, both layers have showed initial failure beyond 25mm deformation. The 600mm layer has totally failed after about 40mm deformation while the 300mm layer was able to increase its load carrying capacity due to remoulding response.

From the predictions of the plane strain model for a wheel load of 500kN (representing a 25t axle load subjected to a dynamic load factor of 4.0), the lower bound deformations obtained were 13mm and 17.5mm for 300 and 600mm layers respectively as shown in Fig. 6.8 (a). At the corresponding upper bound the deformations obtained were 5.0mm for the 300mm layer while for the 600mm layer it was about 6.5mm depicted from Fig. 6.8(b). The margin between the deformations of 300 and 600mm layers was higher at the lower bound (4.5mm) compared to that of the upper bound (1.5mm). This shows that if good quality stiffer materials are used for a capping layer, the ability to withstand settlements is much enhanced irrespective of their layer thicknesses, 300 or 600mm, at normally expected dynamic loading conditions.

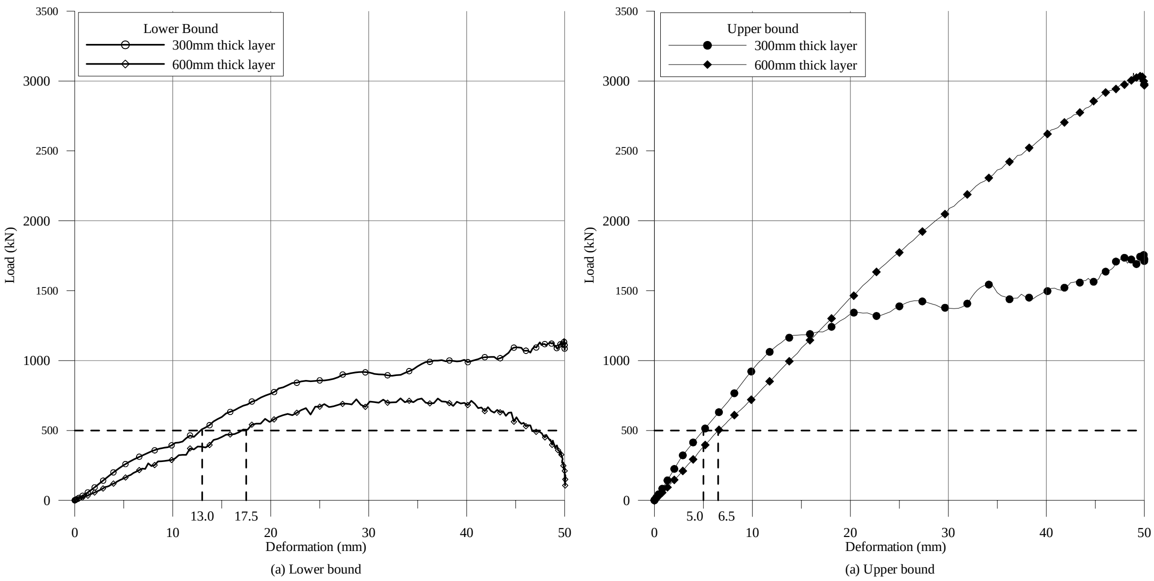

Figure 6.8 Plane strain model predictions and deformations at a 500kN wheel load

In service conditions for railway practices the allowable deformations are usually about 20mm. As shown in Fig. 6.9 (a), at a deformation of 20mm the limit loads obtained for the lower bound were 755kN for the 300mm layer and 565kN for the 600mm layer. At the upper bound the limit loads obtained were 1330kN and 1445kN for 300mm and 600mm layers respectively (Fig. 6.9 (b)). These wheel loads correspond to very high dynamic impact factor and might not be experienced in practice. However a progressive accumulation of damage leading to 20mm deformation at much lower levels of load would be possible; a fatigue analysis would be required to predict such failures. The margin between the loads obtained for the 300 and 600mm layers from the current analysis were higher for the lower bound (190kN) than for the upper bound (115kN). As discussed before this once again confirms that the higher the quality of the material, the larger is the ability to withstand imposed loads than the less stiff material irrespective of their thicknesses.

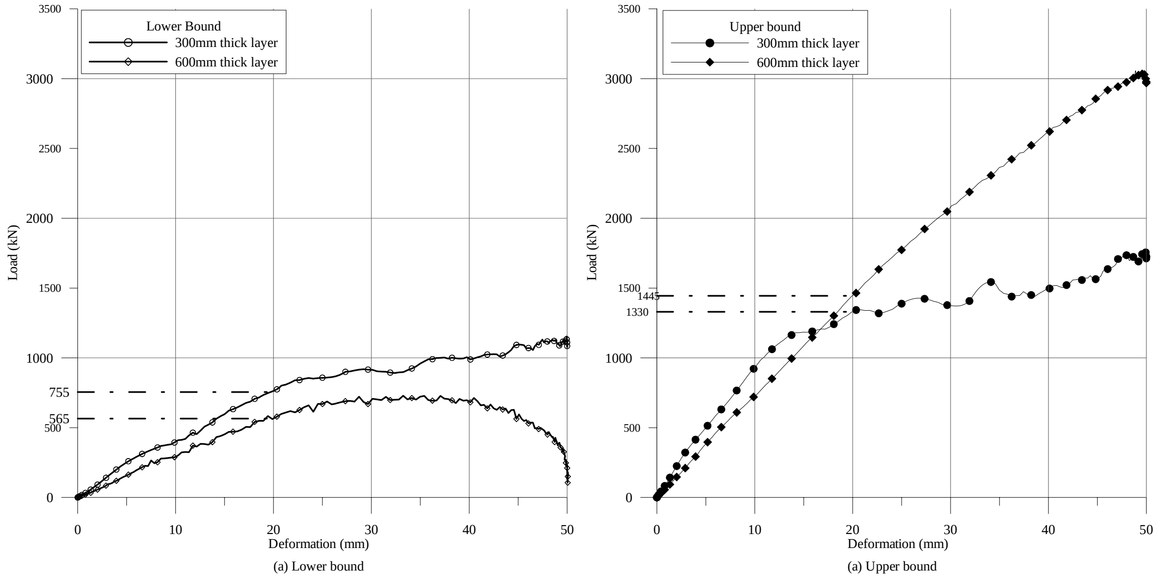

Figure 6.9 Plane strain model predictions and limit loads at a 20mm deformation

Therefore, it can be concluded that if a lower quality (less stiff) material cannot be avoided in the construction of capping layers, a thicker layer would not necessarily be appropriate. However, if a good quality (stiff) material is available then detailed thickness design of the capping layer is less critical. This judgement should be cautiously applied to any practical situations where the boundary conditions are not the same as considered in the limited experimental environment based simulations reported in this thesis. The load-deformation relationship of the capping layer might be significantly affected due to the presence of poor layers below affecting the boundary conditions. Further research would be warranted to examine such effects.

As a general rule it can be concluded that *specifying a good quality material for the capping layer for railway substructure appears more important in practice than improved thickness design criteria or models*. The importance of characterisation of the material advocated in this thesis could be re-emphasised based on this conclusion.

6.4 Validation Experiments

The plane strain FE predictions discussed in the previous section have been validated using full-scale testing. Fig. 6.10 shows the experimental setup.

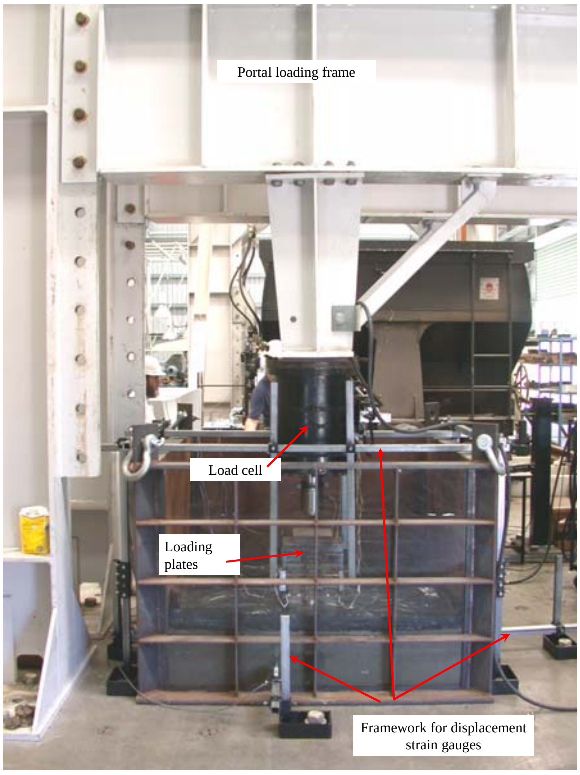

Figure 6.10 Experimental setup

6.4.1 Test Procedure

The axial penetration was imposed by a servo-hydraulic actuator with a load cell (capacity of 2000kN) fitted to a rigid portal frame. The load cell was centred over the capping layer sample and load was transferred via a stack of 50mm thick loading plates as shown in Fig. 6.10. The resisting load to penetration was measured directly via the loading actuator.

The movement of the actuator was also recorded. This is a precautionary measure which is useful in detecting any substantial differences of the movement of the plates to that of the loading actuator that might have occurred during testing.

All instrumentation was connected to separate frames or supports that were independent of the box or loading frame (Fig. 6.10). The strain gauges and displacement transducers located on the bottom loading plate are shown in Fig. 6.11. The average displacement of these displacement transducers was taken as the deformation of the capping layer.

Two sets of displacement transducers were located on the walls of the box to measure any horizontal movements during loading (Fig. 6.10) discussed in Section 6.4. These were located at 150mm height from the top surface of the bottom plate of the box.

To prohibit any substantial amount of moisture loss from the sample after compaction, it was covered with plastic sheets during and after the testing as shown in Fig. 6.11.

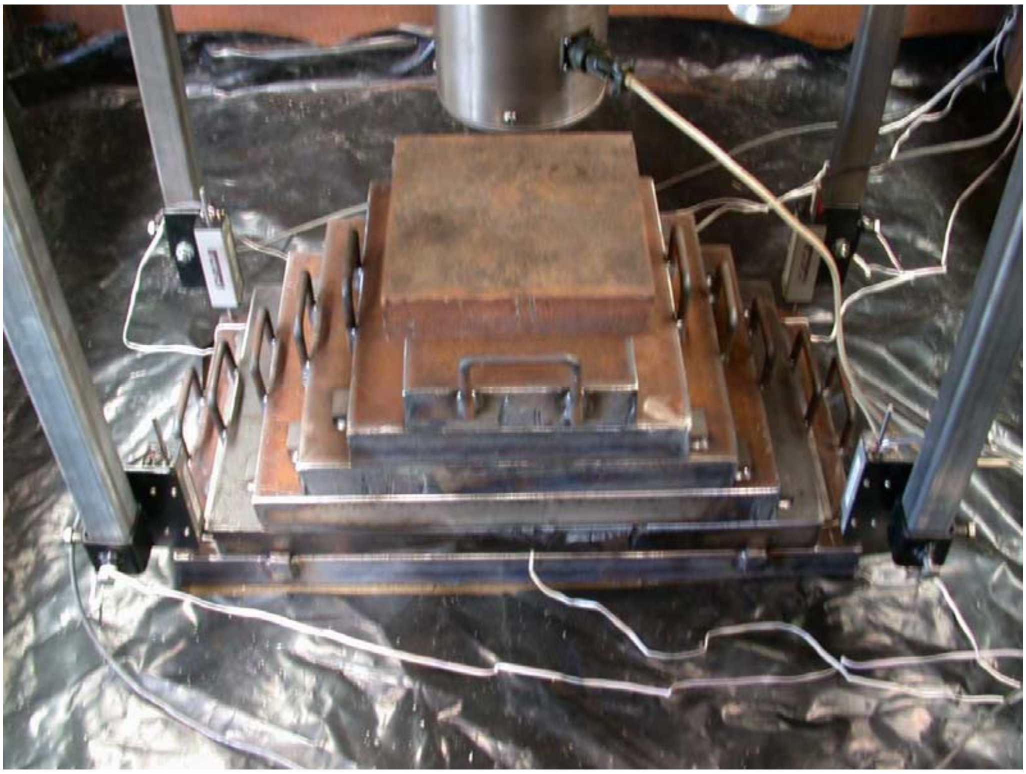

Figure 6.11 Loading plates stack with deformation transducers and strain gauges

The testing procedure is summarised below in detail.

Step 1. The capping layer material was first sieved through a 19mm sieve ensuring that oversize materials were removed. Due to the large material volume (about 8 tons) involved it was sieved through a motor driven sieve as shown in Fig. 6.12.

Step 2. Next, it was mixed using a back hoe at the required moisture level and kept for a minimum of 2hrs allowing water to permeate thoroughly in the mix (Fig. 6.13).

Figure 6.12 Sieving large material volumes using a motor driven sieve

Figure 6.13 Mixing at required moisture level using a back hoe

Step 3. The required compacted layer thickness of 150mm was first marked on the walls of the boxes (Fig. 6.14). The weight of the empty box was recorded as W.

Step 4. To ensure that each layer was of required uniform density, a pre-calculated mass of the required volume was put in to the box and levelled as shown in Fig. 6.14.

Step 5. The layer was then compacted using the 40kg plate compactor (Fig. 6.15) until the required compaction thickness of 150mm was achieved. The specifications of the compactor are plate size 420mm x 292mm, centrifugal force 630kgf (6.2kN), frequency 6200vpm (103Hz), and travel speed 20-22m/min.

Step 6. A layer of chalk dust was then applied on to the surface as shown in Fig. 6.16. This was carried out in each layer with a view to visually observing the deformation profiles after the completion of the test. (However this objective was not realised as samples extracted after testing crumbled without the ability of retaining their shapes.)

Step 7. Once all the required layers were compacted the weight of the box was measured and the density of the compacted sample was obtained. The moisture content of the material used was also measured.

Figure 6.14 150mm thick layers marked on the walls of the box
and a levelled material layer ready for compaction

Figure 6.15 Compaction using a 40kg plate compactor

Figure 6.16 Application of a thin layer of chalk dust

Step 8. Loading plates were then located on the centre of the surface (Fig. 6.17).

Step 9. Next the top surface was covered to minimise evaporation of moisture from the top surface (Fig. 6.18).

Step 10. The box was then centred under the load cell (Fig. 6.19).

Step 11. All the instrumentations were positioned at the required locations (Fig. 6.20).

Step 12. The load was applied at a deformation rate of 5mm/min and the load-displacement data were acquisitioned.

Figure 6.17 Centred loading plates

Figure 6.18 Covered top surface hindering moisture evaporation

Figure 6.19 Centred sample under the load cell ready for instrumentation

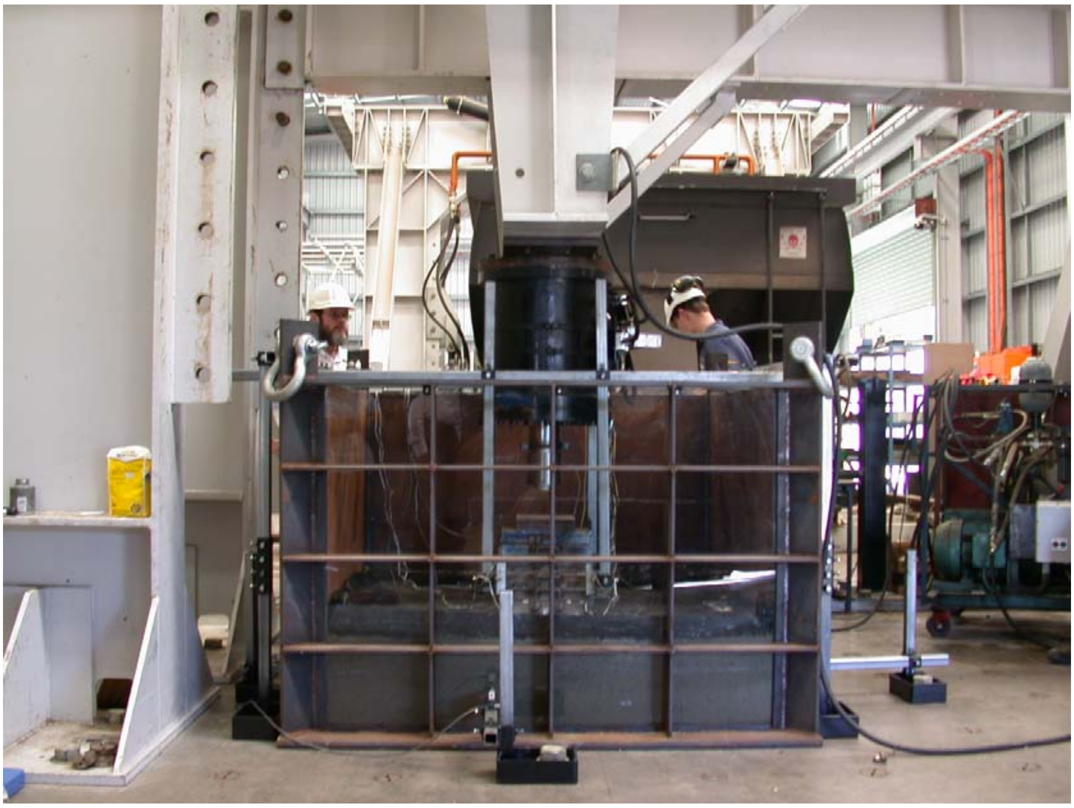

Figure 6.20 Instrumented setup ready for testing

Step 13. At the completion of the test, density of the samples was recorded using a Surface Moisture-Density Gauge (SMDG) as shown in Figs. 6.21 and 6.22.

Step 14. With a view of obtain a deformation profile, some core samples along the centre line of the specimen were obtained (Fig. 6.23).

(a) Using scraper plate/drill rod guide to prepare the test site and aiding the drill rod into the soil

(b) Drilled holes layout ready for taking measurements of density

Figure 6.21 Preparation for the Moisture-density gauge measurement taking

(a) The source rod containing Cesium-137 (8mCi/0.3GBq) is lowered to the desired depth

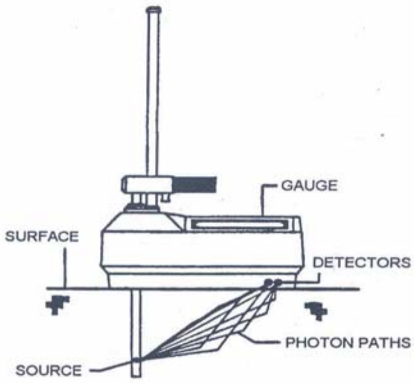

(b) The detectors in the gauge base measure the radiation emitted by the source rod and records the density at the specified depth

Figure 6.22 Obtaining the Moisture-density gauge measurement from SMDG (Troxler Electronic Laboratories Inc 1990-2001)

Figure 6.23 Obtaining core samples along the centre line of the specimen using a 50mm diameter sampler

6.4.2 *Failure Mechanism*

Fig. 6.24 (a) shows how the sample was heaved and moved towards the walls of the box when subjected to vertical penetration. In practice similar behaviour occurs on an operating railway as soil mass is subjected to many thousands of loading, unloading and re-loading cycles as well as repetitive wetting and drying. Such movements may not readily be visible due to the presence of the ballast layer. Instances when water is trapped within the soil mass often cause heaving at the edge of ballast which make visible such movements (Fig. 6.24(b)). Therefore, it can be stated that the application of the load will cause movement of the soil mass not only in the vertical direction (z direction, Fig. 6.1) but also in the horizontal direction (y direction, Fig. 6.1) until equilibrium is achieved. The movements in the longitudinal direction (x direction, Fig. 6.1) will be less prominent.

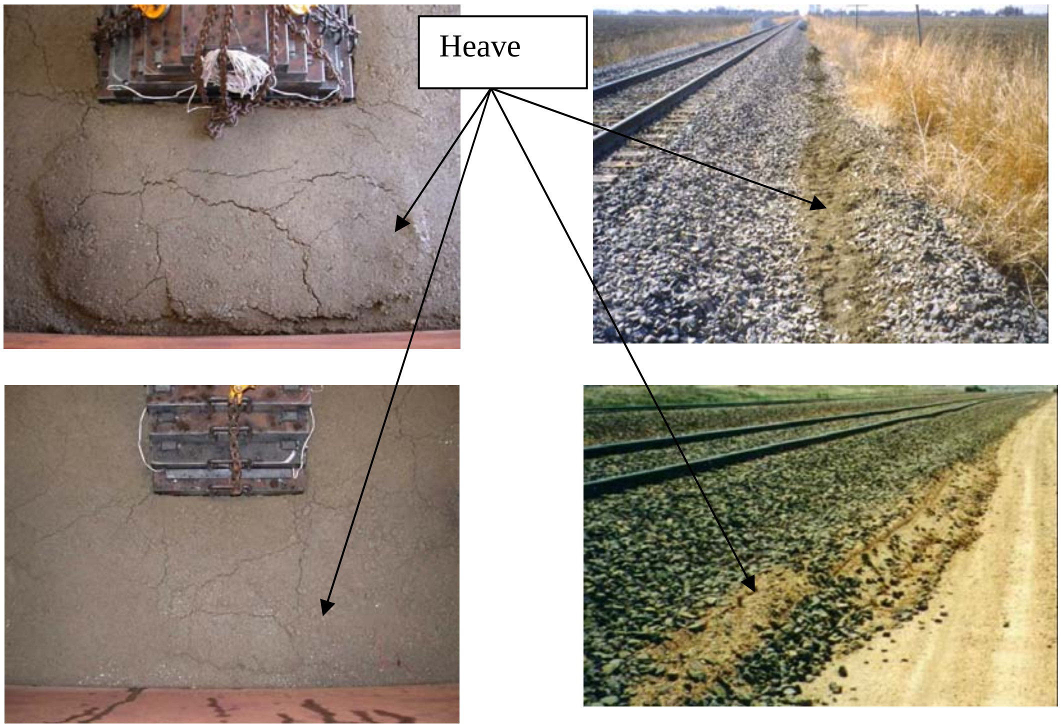

(a) in experiments (b) in practice

Figure 6.24 Heaving and pushing of material due to applied loading

6.4.3 *Deformations and Strains*

The data obtained from the displacement transducers (D_1, D_2, D_3 and D_4) and strain gauges (S_1, S_2, S_3, S_4, S_5 and S_6) located on the loading plate (Fig. 6.3) of the two tests is plotted against the load in Fig. 6.25. The relevant experimental data are located in Appendix D.3.

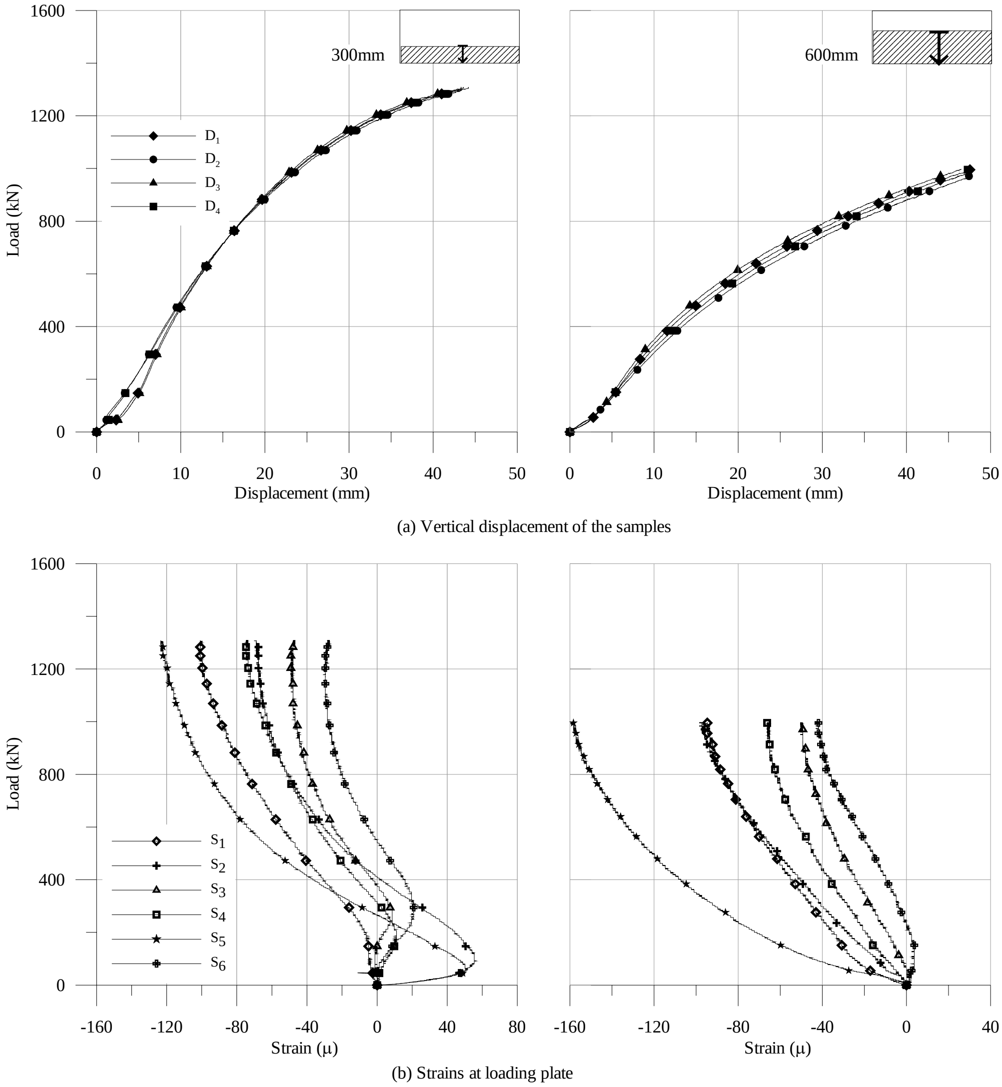

Figure 6.25 Displacement transducer (D_1-D_4) and strain gauge (S_1-S_6) readings relative to the normal load applied on the plate

It can be seen that the displacement transducers D_1-D_4 in the 300mm thick sample test showed almost the same deformation throughout, though below 10mm some discrepancies were observed. This might have been caused by some bedding errors between the load plates and the sample top surface. This is also highlighted in the strain gauge readings S_1-S_6 showing tensile strains (+) induced by the normal force below a load of 400kN. Subsequently all strain gauges showed compressive strains (-) induced by the normal force showing a uniform contact between the plates and the soil. In the 600mm thick sample test the bedding errors were minimal below 400kN as observed in the strain gauge readings S_1-

S_6. The deformation transducers, D_1-D_4 also gave similar results showing parallel movements in relation to each other.

Fig. 6.26 shows the relative movement of the side walls from their original position with load at 150mm from the base top surface as indicated in Fig. 6.2. The steel walls showed movement of less than 1.0mm for 300mm layer and less than 2.0mm for 600mm layer. The polycarbonate sheet wall moved by a maximum of just under 6.0mm.

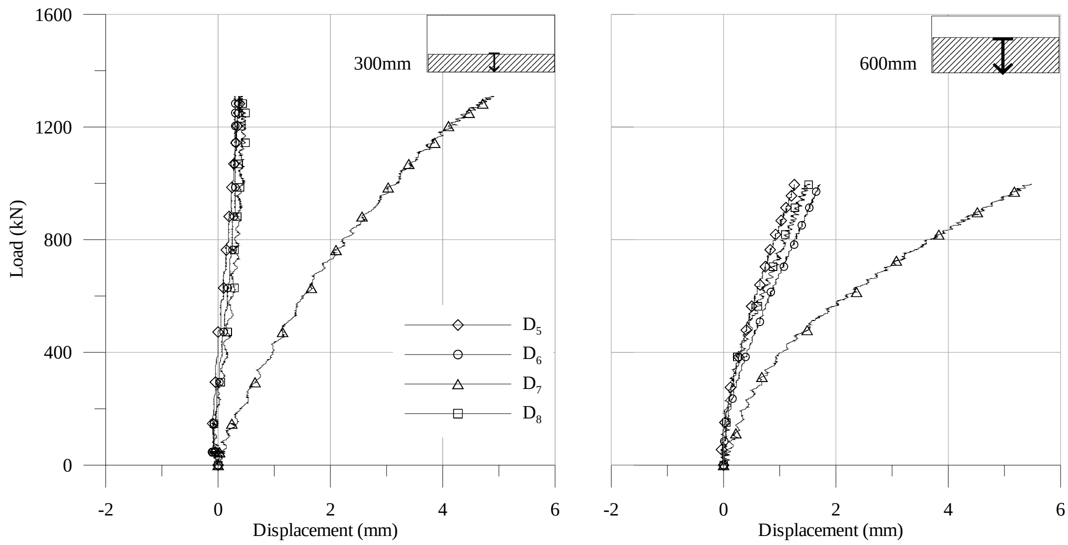

Figure 6.26 Vertical displacement profiles of the side walls

The behavioural pattern of the polycarbonate sheet indicates the flexibility required in the out-of-plane direction of the plane strain specimens (both 300 and 600mm) has indeed been achieved. Movable steel walls have been designed for ballast testing in plane strain conditions by Ionescu et al (2004) which is considerably more complex than the box described in this thesis. The steel wall (measuring in-plane deformation in the lateral direction) movement warranted adjusting the lateral boundary conditions of the vertical faces of the specimens (Figs. 6.5 and 6.6). Spring elements of various stiffness were attached and simulations repeated. No significant difference to the global behaviour of the specimens were observed and hence the work is not reported.

6.4.4 Spatial Variation of Density

Table 6.3 shows the in-situ density of the compacted samples and moisture content of the mix used. The density measurements were obtained by weighing the samples as at the completion of compaction.

Table 6.3 Density and moisture content of the layers

Layer thickness (mm)	300	600
In-situ bulk density (t/m^3)	2.20	2.21
Moisture content (%)	6.3	6.3

By considering the density of the compacted samples before testing it can be stated that overall an average compaction of 95% of the maximum dry density of 2.31t/m^3 (Table 3.1) was achieved by the compaction. This is well within the in-practice specification of 95% modified compaction. After testing, the density is expected to vary spatially and this has occurred as shown in Fig. 6.27 where the data measured by the Surface Moisture-Density Gauge (SMDG) at the completion of the tests are presented. Using the SMDG the densities were recorded at a depth of 150mm from the surface. Fig. 6.27 shows the densities within the loaded area and its outskirts. As expected, it was observed that the density within the loaded areas were higher than that of the outskirts.

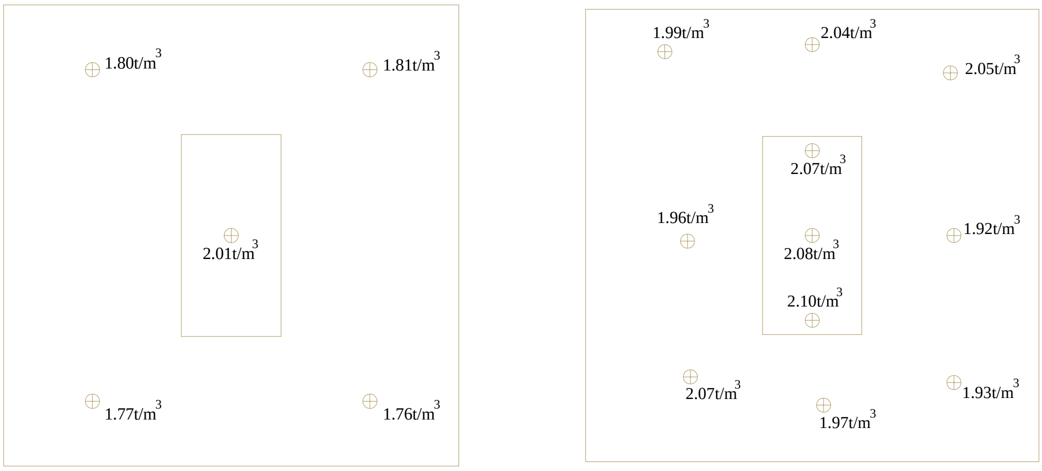

(a) 300mm layer (b) 600mm layer

Figure 6.27 Dry density recordings obtained from SMDG

The average modified compaction of the 300mm layer within the loading plate area was 87%. In the 600mm layer an average modified compaction of 90% had been achieved. The average modified compaction of the outskirts of the loaded area was 79% (300mm layer) and 86% (600mm layer). The reduction in the densities were obvious at a level of 150mm below the top surface as already the application of load has caused failure of the sample, loosened due to tensile stresses as shown in Fig. 6.24 (a).

Core sample data

Though the core samples were obtained (Fig. 6.23) with the view of obtaining the deformed profile, they were unable to be removed properly from the sampler without disturbing them. In fact, already loosened core samples were not intact and collapsed when removed from the sampler. Therefore, the expected deformed profiles could not be drawn.

6.5 Results and Discussions

Fig. 6.28 shows the final load-deformation profiles obtained from the experiments for capping layer thicknesses of 300 and 600mm. The average of displacement transducers (D_1, D_2, D_3 and D_4) was taken as the total deformation of the sample in the experimental results. It can be seen that a substantial progressive stiffness reduction had occurred with the increase in layer thicknesses. The gradual development of the ultimate load is indicative of progressive failure rather than a sudden brittle failure. This can be described as gradual transfer of load from failed zones to unfailed zones where the ultimate load will be reached as a combination of failed, nearly failed and other stresses. It is evident from the results that capping layer failures are progressive over a finite area rather than a singular stress value.

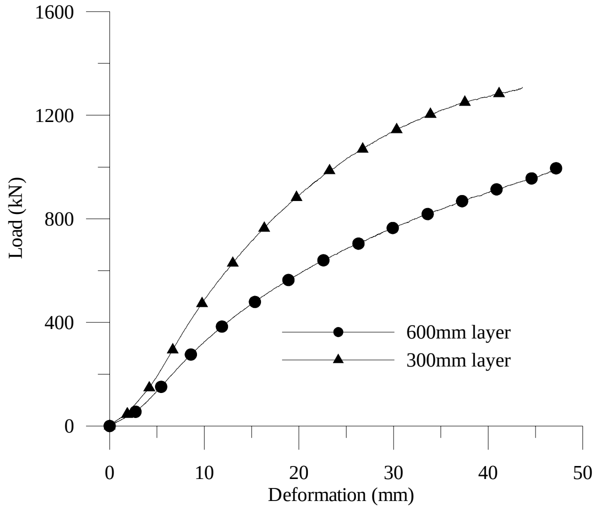

Figure 6.28 Comparison of load-displacement profiles of varying thicknesses

Figure 6.29 shows the experimental results together with the FE simulations carried out using the upper and lower bounds of the SCT predictions. It can be seen from the graphs that the experimental predictions tend towards the very extreme to the lower bound. Given the variability in the properties of the soils like the capping layer material considered in this thesis, the ability of the FE model to predict the capping layer material behaviour under plane strain conditions using constitutive properties obtained from axisymmetric FE modelling based backcalculation method coupled with SCT, is considered satisfactory.

Furthermore, although the properties of the capping layer material have been obtained from specimens under high levels of confining stresses, the constitutive material modelling developed in this thesis based on Drucker-Prager theory of plasticity including pressure dependent tangent modulus and angle of friction has worked well in adapting itself for situations that are vastly different to that of the original conditions from which they have been developed. Conversely it could be stated that although material data more representative of the field condition could be obtained by testing the capping layer materials in large boxes under plane strain condition with small levels of lateral confinement, given the costs and time required for such tests, it is reasonable to estimate the properties of the materials using much smaller size specimens (SCT) contained in the CBR mould.

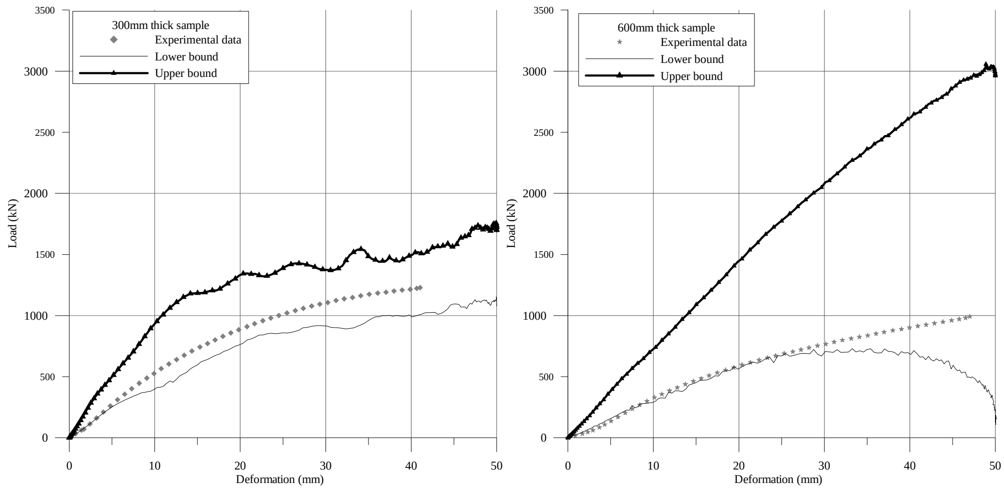

Figure 6.29 Comparison of experimental data with FEM predictions

From the two tests carried out it can be concluded that,

- The SCT predicted material properties were able to simulate the experimental behaviour of the capping layer under different conditions of stress states and FE idealisations.
- By successfully incorporating the pressure dependent tangent modulus and the angle of friction into the constitutive relationship, the model was able to predict the required material properties using the developed small-scale semi confined test which was much easier and economical to perform and less time consuming than cyclic triaxial tests.
- The use of the present model and the limited number of validated experiments does not guarantee that the SCT predictions can be used “generally” for either other materials or significantly different layer thicknesses of capping layer materials.

- The two validation tests had fixed base boundary conditions instead of the in service conditions of underlying soils of variable quality. Therefore, more experimental validation with an underlying layer of soil is required to prove the reliability of the present model in predicting behaviour in actual situations.

6.6 Summary

The development of a new small-scale experimental method (SCT) based FE backcalculation simulations of non-cohesive granular material has been reasonable in predicting the required properties that can be used for in-situ plane strain conditions prevailing in railway substructure and in road pavement. It is proved that data predicted from axisymmetric FE simulations can be successfully applied to plane strain conditions.

Large scale testing of capping layer in a purpose built testing apparatus has proved that the SCT predictions were reasonable and that this inexpensive method can be used as an alternate method to the conventional cyclic triaxial tests that are time consuming and expensive.

The development of a constitutive relationship that accounts for the pressure dependency of the properties of the non-cohesive capping soils has been successfully utilised in predicting material properties as well as permanent deformations based on theory of plasticity, whereas most models developed in past decades incorporated only the theory of elasticity of the material as described in detail in Chapter 2.

Though the limited number of validation tests (two) showed promising results, more experimental data are needed to generalise the findings prior to field applications.